Magnetic Frustration and Iron-Vacancy Ordering in Iron-Chalcogenide

Chen Fang,[1] Bao Xu,[2] Pengcheng Dai,[3,2] Tao Xiang,[2,4] and Jiangping Hu[1,2]

[1] *Department of Physics, Purdue University, West Lafayette, Indiana 47907, USA*
[2] *Beijing National Laboratory for Condensed Matter Physics, Institute of Physics, Chinese Academy of Sciences, Beijing 100080, China*
[3] *The University of Tennessee, Knoxville, Tennessee 37996-1200, USA*
[4] *Institute of Theoretical Physics, Chinese Academy of Sciences, Beijing 100080, China*

We show that the magnetic and vacancy orders in the 122 ($A_{1-y}Fe_{2-x}Se_2$) iron-chalcogenides can be naturally derived from the $J_1-J_2-J_3$ model with J_1 being the ferromagnetic (FM) nearest neighbor exchange coupling and J_2, J_3 being the antiferromagnetic (AFM) next and third nearest neighbor ones respectively, previously proposed to describe the magnetism in the 11(FeTe/Se) systems. In the 11 systems, the magnetic exchange couplings are extremely frustrated in the ordered bi-collinear antiferromagnetic state so that the magnetic transition temperature is low. In the 122 systems, the formation of iron vacancy order reduces the magnetic frustration and significantly increases the magnetic transition temperature and the ordered magnetic moment. The pattern of the 245 iron-vacancy order ($\sqrt{5}\times\sqrt{5}$) observed in experiments is correlated to the maximum reduction of magnetic frustration. The nature of the iron-vacancy ordering may hence be electronically driven. We explore other possible vacancy patterns and magnetic orders associated with them. We also calculate the spin wave excitations and their novel features to test our model.

The recent discovery of a new family of iron-based superconductors, the 122 iron-chalcogenides $A(K,Cs,Rb)_yFe_{2-x}Se_2$[1–3], with a superconducting transition temperature even higher than 40 K has attracted many research attentions. The compounds are heavily electron doped with only electron Fermi pockets which are mainly located at the M point of the unfolded Brillouin zone as shown by both angle-resolved photoemission spectroscopy (ARPES)[4–6] and LDA calculations[7–9]. Among all of iron-based superconductors, the new materials also have the highest magnetic transition temperature around 500K and the largest ordered magnetic moment around $3\mu_b$[10, 11]. The materials are also featured with intrinsic iron vacancies which can order themselves below some transition temperatures[10, 12–16]. Currently, it is unclear how the magnetic, vacancy and superconducting orders are correlated.

For iron-pnicitides, their parental compounds display an universal collinear antiferromagnetic (CAFM) phase[17], which can be described by a simple magnetic exchange model including the nearest neighbor (NN) J_1 (note, in magnetically ordered state, the effective exchange coupling becomes J_{1a} and J_{1b} due to rotation symmetry breaking) and the next nearest neighbor(NNN) J_2[18, 19]. However, for iron-chalcogenides, different magnetic orders have been observed[20, 21]. For example, the 11 iron-chalcogenides, $FeTe_{1-x}Se_x$[22], which can achieve the superconducting transition temperature around 40K under pressure[23], can display both commensurate and incommensurate magnetic state. The ordered magnetic moment of the parent compound $FeTe$ is about $2.0\mu_b$, significantly larger than iron-pnictides as well. Recently, it has been shown that the magnetic state of $FeTe$, which is a bi-collinear antiferromagnetic (BAFM) can be described by a strongly frustrated magnetic model including the nearest neighbor (NN) J_1, the next nearest neighbor(NNN) J_2 , and the third nearest neighbor (TNN) J_3, i.e. the $J_1-J_2-J_3$ model[24, 25]. It has been determined that J_1 is ferromagnetic (FM) while J_2 and J_3 are antiferromagnetic (AFM)[26]. It is also interesting to note that in the BAFM state, the J_1 effectively becomes J_{1a} and J_{1b} due to symmetry breaking, which also help to stabilize the BAFM phase. The values of the magnetic exchange coupling parameters suggest that FeTe is close to a boundary between an incommensurate magnetic phase and the BAFM phase so that the later can lose its stability by an introduction of a few percentages of additional Fe atoms[20].

However, it is still hotly debated about whether the effective models with local magnetic exchange couplings are the right models to describe the magnetism in iron-based superconductors. For iron-pnictides, there is less debate since the model is simple and has gained support from different families of iron-pnictides. However, for $FeTe$, the model lacks of independent verification. Since the local physics of the 122 iron-chalogenides should be similar to the one of $FeTe$, it is naturally expected that both families of iron-chalogenides should be described by similar models.

In this paper, we show that the magnetism in both families of iron-chacogenides can be unifiedly understood within the previous model obtained for $FeTe$. The 245 ($K_2Fe_4Se_5$) pattern ($\sqrt{5}\times\sqrt{5}$) of the vacancy orders in the 122 system are naturally obtained by maximizing the magnetic energy saving and reducing the magnetic frustration in the model. The magnetic order in the 122 systems becomes robust and the ordered moment is significantly enhanced. The magnetic transition temperature

around 500k of $K_2Fe_4Se_5$ quantitatively agrees with the pure magnetic energy gain, comparing to the magnetic transition temperature around 70K in $FeTe$ where the magnetic frustration is strong. Therefore, the vacancy ordering may be originated electronically. We explore other possible vacancy patterns and magnetic orders associated with them. Moreover, we calculate spin wave excitations and identify their novel features to quantitatively test the proposed theory.

Before we start to consider the effect of vacancy, let's review the $J_1-J_2-J_3$ model, which was used to describe the magnetism in $FeTe$[24, 25]. The Hamiltonian is given by

$$H = \sum_{\alpha} J_{\alpha} \sum_{<ij>_{\alpha}} S_i \cdot S_j \tag{1}$$

where $\alpha = 1, 2, 3$. The BAFM state in FeTe, which breaks the rotation symmetry, is stabilized with a coupling to the small lattice distortion. In the BAFM state, this broken symmetry can generate the anisotropy among J_1 and J_2 couplings. For $FeTe$, by fitting the spin wave spectrum, we have obtained the values of the magnetic exchange couplings with $J_1S \sim -34mev$, $J_2S \sim 22mev$ and $J_3S \sim 7mev$[26], where S is the spin of each site. The anisotropy is shown mainly in J_1, with $\frac{J_{1a}-J_{1b}}{2} \sim -16mev$[26]. The most important feature revealed from the fitting is that the NN coupling J_1 is FM while the other two, J_2 and J_3, are AFM. The sum of these three coupling parameters is close to zero, which indicates the model is extremely magnetically frustrated.

Let's first ignore the anisotropy of the magnetic exchange coupling J_1 caused by symmetry breaking in the BAFM state. We focus on the pure magnetic model in the tetragonal square lattice. In the BAFM state as shown in fig.1, both J_1 and J_2 are frustrated couplings and the magnetic energy is only saved by J_3. The saved magnetic energy per site is given by $E_{BAFM} = -2J_3S^2$. Now, we ask a simple question, what are the possible stable magnetic orders if we can remove spins and form vacancy patterns in the above model within the similar parameter regions? (note, in the following we will take $S = 1$ for convenience.)

In order to create a vacancy pattern that minimizes the magnetic exchange energy, the pattern must sufficiently suppress magnetic frustration and maximize energy saving from each magnetic exchange coupling simultaneously. It is straightforward to show that such a pattern is exactly the 245 pattern (named according to $K_2Fe_4As_5$) as shown in fig.2, which has been identified by neutron scattering experiments[10]. In the 245 vacancy orders, each site has three NN and NNN couplings to its neighbors. Moreover one spin in each connected five spins (5-1 pattern) along Fe-Fe direction is removed. The odd number of links for both NN and NN couplings reduce the magnetic frustration completely. The 5-1 pattern saves energy from J_3 as well.

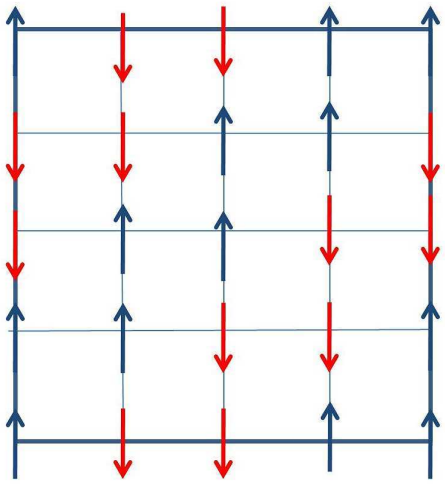

FIG. 1: The bi-collinear antiferromagnetic phase observed in the 11 (FeTe/Se) systems.

Therefore, the 245 state maximizes the energy saving from all magnetic exchange couplings. The magnetic energy saving per spin $E_{245} = (-J_1 + J_2 + 2J_3)/2$(we set $J_3 = 0$ between two NNN sites if there is vacancy between them). If we ignore the lattice distortion and use the exchange parameters derived from $FeTe$, $E_{245} \sim 70mev$, comparing to $E_{BAFM} \sim 14mev$. Considering the fact that the ordered magnetic moment is also around 1.5 times larger in $K_2Fe_4As_5$ than in $FeTe$, the ratio of the magnetic energy savings between two states is given by $1.5 \times E_{245}/E_{BAFM} \sim 7.5$. This ratio is in a quantitative agreement with the ratio of their magnetic transition temperatures $500k/70k \sim 7.1$. (Note: in general, the magnetic transition temperature in a quasi two dimensional material is given by $T_N \propto \frac{E}{ln\frac{E}{J_c}}$, where J_c is the coupling strength between layers and E is the in-plane magnetic energy saving.) The vacancy pattern is hence a result of the combination of energy saving from three magnetic couplings including the large contribution from the NN ferromagnetic exchange coupling. If we consider the symmetry breaking of the state which can modify the magnetic coupling strength as shown in fig.2, the total energy saving in general can be written as $E'_{245} = (-2J_1 - J'_1 + 2J'_2 - J_2 + 2J_3 - J'_3)/2$ where the parameters are defined in fig.2.

It is also interesting to explore other possible vacancy patterns and their associated magnetic orders. For such an frustrated $J_1 - J_2 - J_3$ magnetic model, there is no other pattern, except the 245 ordering, which can get rid of the magnetic frustration completely. With the values of the exchange couplings given above, we list some pos-

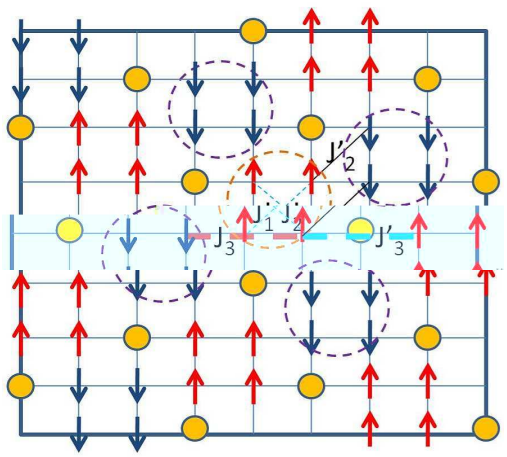

FIG. 2: The sketch of the 245 vacancy ordering and its magnetic structure. The general magnetic couplings are also indicated.

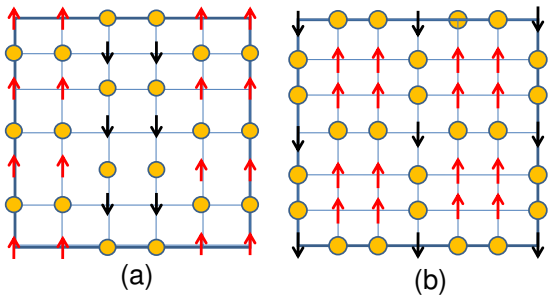

FIG. 3: (a) The armchair dimer crystal pattern. (b)The square dimer crystal pattern.

sible patterns (we again set $J_3 = 0$ between two NNN sites if there is vacancy between them): (1) Armchair dimer crystal patterns (the 212 pattern if we consider K_2FeSe_2) shown in fig.3(a). In this pattern, half of spins are replaced by vacancies. The magnetic energy saving per site is given by $E_{ADC} = J_2 - J_1/2$. The pattern saves both energy from the NN FM and NNN AFM couplings; (2) Square dimer crystal patterns shown in fig.3(b). The energy saving from this structure stems from the NN FM J_1 and the NNN AFM J_2, $E_{SDC} = \frac{-4J_1+2J_2}{5}$; (3) The 234 vacancy patterns (named as $K_2Fe_3Se_4$) as shown in fig.4. There are two different patterns. The first pattern saves energy from J_1 and J_2 but pays energy cost for J_3. The energy saving per site is given by $E_{234a} = -J_1/3 + 2J_2 - 2J_3$. This magnetic structure is

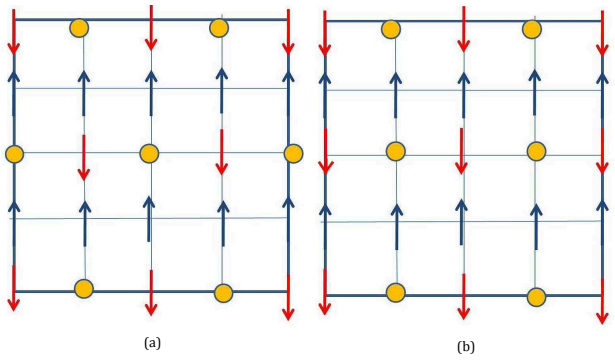

FIG. 4: The two different possible patterns (234) for $Fe_{1.5}Se_2$.

similar to the $(0, \pi)$ collinear AFM (CAFM) observed in the parental compounds of iron-pnictides. In the second pattern, the magnetic state is also similar to CAFM. The energy saving is given by $E_{234b} = \frac{4}{3}(J_2 - J_3/2)$. In general, the 234 phase where the iron concentration is close to 1.5 is most likely supporting a CAFM magnetic phase, similar to iron pnictides. In both patterns, there are ferromagnetic moments for each layer. Between layers, they are antiferromagnetically coupled. The 234 vacancy patterns have been observed experimentally[28]. However, the magnetic order has not been identified. (4) The 446 pattern ($K_4Fe_4Se_6$) as shown in fig.5. There are also two possible patterns. The first pattern is a dimer vacancy ordering. The magnetic pattern is also close to CAFM phase with an energy saving given by $E_{234a} = \frac{J_2 - J_3 - 3J_1}{4}$. The second pattern can be viewed as a diagonal stripe similar to undoped cuprates[29]. For such a stripe pattern, there is no J_3 coupling. The magnetic structure can be predicted to be incommensurate along the stripe direction and AFM along the direction perpendicular to the stripe. The total energy saving per site is given by $E_{446} = \frac{3}{2}J_2 + \frac{J_1^2}{8J_2}$. The spin angle between two NN sites along the stripe direction is given by $cos\theta = -\frac{J_1}{4J_2}$.

Properties of the 245 state in the large S limit: The 245 state is clearly the most stable magnetic state in our model. In the following, we focus on this state. First, we analyze the spin excitation in the large S limit. We consider a general model as shown in Fig.2. To start a spin wave calculation, we denote the spin sites as follows. A generic position of the spin is given by $\mathbf{r} = m\mathbf{l_1} + n\mathbf{l_2} + \mathbf{d_i}$, where m, n are integers and $\mathbf{l_1} = (2\mathbf{x} - \mathbf{y})/\sqrt{5}, \mathbf{l_2} = (\mathbf{x}+2\mathbf{y})/\sqrt{5}, \mathbf{d_1} = 0$, $\mathbf{d_2} = \mathbf{x}$, $\mathbf{d_3} = \mathbf{x}+\mathbf{y}$, $\mathbf{d_4} = \mathbf{y}$, where $\mathbf{x}, \mathbf{y}$ are unit vectors in the original tetragonal lattice. We take the Holstein-Primakoff transform for the given ground state:
For $m + n$ =even:

$$S_+(\mathbf{r}) = \sqrt{2S}a_i(\mathbf{R}), \quad (2)$$

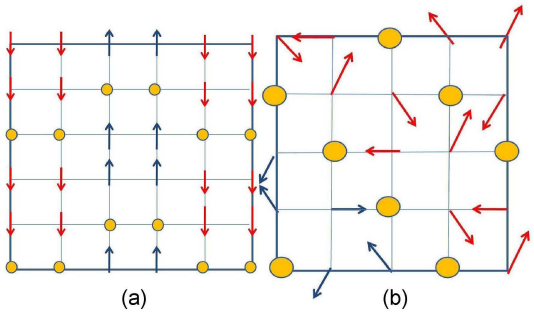

FIG. 5: The two different possible patterns for $Fe_{1.33}Se_2$: (a) The dimer vacancy ordering similar to CAFM magnetic phase. (b) The diagonal stripe pattern where the magnetic ordering is incommensurate.

$$\begin{aligned} S_-(\mathbf{r}) &= \sqrt{2S}a_i^\dagger(\mathbf{R}), \\ S_z(\mathbf{r}) &= S - a_i^\dagger(\mathbf{R})a_i(\mathbf{R}); \end{aligned}$$

For $m+n$ =odd:

$$\begin{aligned} S_+(\mathbf{r}) &= \sqrt{2S}a_i^\dagger(\mathbf{R}), \\ S_-(\mathbf{r}) &= \sqrt{2S}a_i(\mathbf{R}), \\ S_z(\mathbf{r}) &= -S + a_i^\dagger(\mathbf{R})a_i(\mathbf{R}). \end{aligned} \tag{3}$$

The full Hamiltonian of the model can be put in a matrix form. Define $\psi^\dagger(k) = (a_1^\dagger(k), a_2^\dagger(k), a_3^\dagger(k), a_4^\dagger(k), a_1(-k), a_2(-k), a_3(-k), a_4(-k))$, and we have

$$H = \frac{1}{2}\sum_k \psi^\dagger(k) \begin{pmatrix} A(k) & B(k) \\ B(k) & A(k) \end{pmatrix} \psi(k). \tag{4}$$

$A(k)$ and $B(k)$ are four-by-four matrices, defined by:

$$A(k) = S \begin{pmatrix} E_0 & J_1 e^{ik_x} & J_2 e^{ik_x+ik_y} + J_3' e^{-i2k_x} & J_1 e^{ik_y} \\ \cdot & E_0 & J_1 e^{ik_y} & J_2^{-ik_x+ik_y} + J_3' e^{-2ik_y} \\ \cdot & \cdot & E_0 & J_1 e^{-ik_x} \\ \cdot & \cdot & \cdot & E_0 \end{pmatrix}, \tag{5}$$

$$B(k) = S \begin{pmatrix} 0 & J_2' e^{-ik_x+ik_y} + J_3 e^{-2ik_y} & J_1' e^{-ik_y} & J_2' e^{-ik_x-ik_y} + J_3 e^{2ik_x} \\ \cdot & 0 & J_2' e^{-ik_x-ik_y} + J_3 e^{2ik_x} & J_1' e^{ik_x} \\ \cdot & \cdot & 0 & J_2' e^{ik_x-ik_y} + J_3 e^{2ik_y} \\ \cdot & \cdot & \cdot & 0 \end{pmatrix}, \tag{6}$$

where $E_0 = -2J_1 - J_2 + J_1' + 2J_2' + 2J_3 - J_3'$. The lower triangle elements are suppressed because both matrices are hermitian.

By diagonalizing this Hamiltonian, we have

$$H = \sum_{i=1,2,3,4;k} (\gamma_i^\dagger(k)\gamma_i(k) + 1/2)\omega_i(k), \tag{7}$$

and

$$a_i(k) = \sum_j U_{ij}(k)\gamma_j(k) + V_{ij}(k)\gamma_j^\dagger(-k). \tag{8}$$

where U and V are 4×4 matrices to diagonalize the Hamiltonian. The spin reduction due to quantum fluctuations on each site is given by:

$$\delta m = \frac{1}{4\pi^2}\sum_j \int_0^{2\pi} dk_x \int_0^{2\pi} dk_y |V_{1j}(k_x,k_y)|^2. \tag{9}$$

It is also interesting to calculate the dynamic factor $S(\omega) = -\Im[\chi(\omega)]$, where the local susceptibility $\chi(\omega)$ is defined as

$$\chi(i\omega_n) = \sum_q \int d\tau e^{i\omega_n\tau}[\langle S^+(q,\tau)S^-(-q,0)\rangle + \langle S^-(q,\tau)S^+(-q,0)\rangle]/N. \tag{10}$$

After taking Fourier transform, we obtain

$$\chi(\omega) = \sum_k \sum_{i,j} (|V_{i,j}(k)|^2 + |U_{i,j}(k)|^2) \left(\frac{1}{\omega - E_j(k) + i0} + \frac{1}{\omega + E_j(k) + i0}\right)/N. \tag{11}$$

Due to the enlarged unit cell, the spinwave BZ (SBZ) is smaller than the original unfolded BZ for one Fe per unit cell. The SBZ is cornered by the following four (equivalent) points $(-3\pi/5, -\pi/5)$, $(\pi/5, -3\pi/5)$, $(3\pi/5, \pi/5)$, and $(-\pi/5, 3\pi/5)$, and these points are called M_s points, different from the real M point in lattice BZ. It is convenient to define $X_s = (2\pi/5, -\pi/5)$ and $Y_s = (-\pi/5, -2\pi/5)$ for future discussion. The

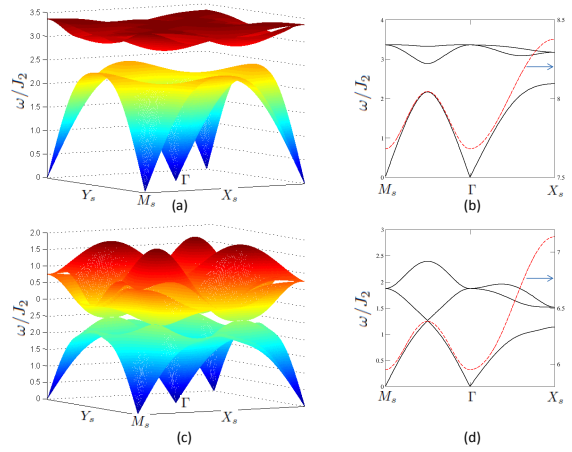

FIG. 6: The spinwave spectra of the lowest three branches (the other one is too high to be drawn in the same plot) using the parameters $(J_1, J_1', J_2, J_2', J_3, J_3') = (-30, -10, 20, 20, 9, 0)$meV in (a) and $(J_1, J_1', J_2, J_2', J_3, J_3') = (-30, -30, 20, 20, 9, 0)$meV in (b). The corresponding band structures are given in (b) and (d), in which the read dashed lines represent the highest branch and black solid lines the lowest three branches. M_s, X_s and Y_s are high symmetry points in the spinwave BZ that are defined in text.

spinwave has four branches. Depending on the parameters, there can be finite gaps between the first and the second branches and between the third and the fourth ones . The middle two branches are degenerate at Γ and M_s points and are in general close to each other. At high symmetry points, the spinwave energy has analytic expressions. We take $S = 1$ for convenience. At M_s and Γ: $E_1(\Gamma) = 0, E_2(\Gamma) = E_3(\Gamma) = 2\sqrt{(J_e - J_1 - J_2 - J_3')(J_1' - J_1 - J_2 + J_e - J_3')}$, and $E_4(\Gamma) = 2\sqrt{2}\sqrt{(J_1' - 2J_1)(J_e - J_1)}$ where $J_e = J_2' + J_3$ are the effective antiferromagnetic coupling strength between two 4-spin plaquettes. At X_s, $E_1(X_s) = 2(J_1 + \sqrt{(J_e - J_3' - J_1)(J_1' + J_e - J_3' - J_1)}), E_2(X_s) = 2\sqrt{J_1^2 + (J_2 - 2J_2')(J_2 - 2J_3) + \omega}$, where $\omega = J_1'(J_e - J_2) - J_1(J_1' + 2J_e - 2J_2)$, and $E_4(X_s) = 2(-J_1 + \sqrt{(J_e - J_3' - J_1)(J_1' + J_e - J_3' - J_1)})$, which also defines the spinwave band width. The first spinwave branch effectively describes the spin fluctuations of 4-spin plaquettes.

We calculate spinwave spectra and related features for three different parameter sets. We first adopt the parameters: $J_1 = (J_{1a} + J_{1b})/2 = -30$meV, $J_2 = 20$meV, $J_3 = 9$meV. Due to lattice distortion that draws the four spins in each new unit cell closer, the primed parameters can be reduced from unprimed ones by the presence of iron vacancies: $J_1' = -10$meV, $J_2' = 20$meV and $J_3' = 0$meV. For these parameters the spinwave spectra have a finite gap $\Delta_{12} = 10.2$meV between the first and the second branches, and a larger gap $\Delta_{34} = 86.2$meV between the third and fourth branches. The full bandwidth is $W = 167.5$meV. The first branch starts from zero energy at Γ and M_s and reaches maximum at X_s; the second and third branches start from minimum at $(3\pi/10, \pi/10)$ and its three C_4 equivalents, and reach maximum at $(0.45\pi, 0.12\pi)$. The fourth branch starts from $E_4(\Gamma)$ at Γ and M_s to $E_4(X_s)$ at X_s. The ordered moment correction from spinwave is $\delta m = 0.095$. See Fig.6(a,b) for details.

In choosing the second parameter set, we consider a purely magnetic model without lattice distortion. Therefore we take $J_1' = J_1$, $J_2' = J_2$. However one still has $J_3 \gg J_3' \sim 0$ because of the vacancy along the exchange path for J_3'. For this parameter set, there is no gap between the first and second branches, but the gap between third and fourth branch remains finite. The full bandwidth in this case is $W = 142.7$meV. The first three branches start from zero energy at Γ and M_s, and reach maximum at $(3\pi/10, \pi/10)$ and its three C_4 equivalents. The fourth branch's minimum and maximum appear at the same points as in the first parameter set. The ordered moment correction from spinwave is $\delta m = 0.197$. See Fig.6(c,d) for details.

In FeTe, we found that the third neighbor exchange J_3 is needed to explain both low and high energy regions of dynamic spin susceptibility observed in neutron experiment, while a parameter fit without J_3 significantly underestimates the spin wave bandwidth. J_3 is also important in the current system to stabilize the 245 state. For comparison, we adopt the parameters we used to fit FeTe system without J_3 (see supplementary materials in Ref.[26]): $(J_1, J_1', J_2, J_2', J_3, J_3') = (-12, -4, 9, 9, 0, 0)$meV. The spinwave correction to moment in this case is $\delta m = 0.43$, indicating much stronger spin fluctuation.

The dynamic factor is shown in Fig.7. Note that around zero energy the dynamic factor should drop to zero in a 3D system, but converge to a finite value in our 2D system. If we include a small J_z in the beginning, we can make the curve drop to zero at zero energy, however the dynamic factor at $\omega \gg J_z$ is unaffected. See Fig.7 for the dynamic factor with all three parameter sets given above.

It is also interesting to check what is the closest magnetic state if the exchange coupling parameters can be varied in the 245 state. In the reasonable parameter space, the following states can be considered: 1. The ferromagnetic state if J_1 and J_1' are large. 2. the CAFM state when J_2 is large. 3. The incommensurate phase. The ground state energy for the first two are easy to calculate: $E_{FM} = 4J_1 + 2J_1' + 2J_2 + 4J_2' + 4J_3 + 2J_3'$ and $E_{AFM2} = -2J_2 - 4J_2' + 4J_3 + 2J_3'$. Comparing the energies, we have if $|J_1'| > 2(J_2' + J_3)$, the FM phase wins over the 245 magnetic phase; and if $2|J_1| - |J_1'| < 2J_2 - 4J_3$, CAFM state has lower energy than the 245 magnetic state and thus becomes preferable. Most importantly, an ICM state is the closest competitor to the 245 magnetic

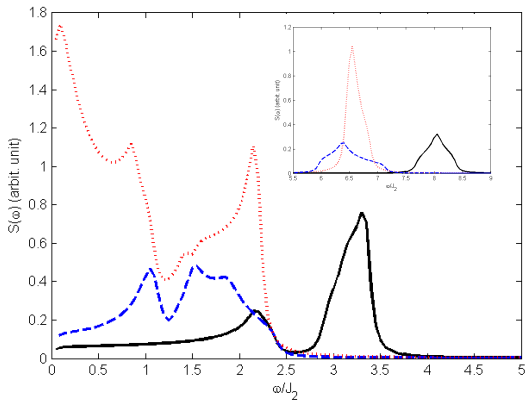

FIG. 7: The dynamic factor $S(\omega)$ contributed by spinwave. Black solid line corresponds to $(J_1, J_1', J_2, J_2', J_3, J_3') = (-30, -10, 20, 20, 9, 0)$meV; blue dashed line corresponds to $(J_1, J_1', J_2, J_2', J_3, J_3') = (-30, -30, 20, 20, 9, 0)$meV; and red dotted line $(J_1, J_1', J_2, J_2', J_3, J_3') = (-12, -4, 9, 9, 0, 0)$meV. The main panel only includes contribution from lowest three branches as the highest branch is too high to be plotted in a same energy range. The inset shows the contribution by the fourth and highest branch.

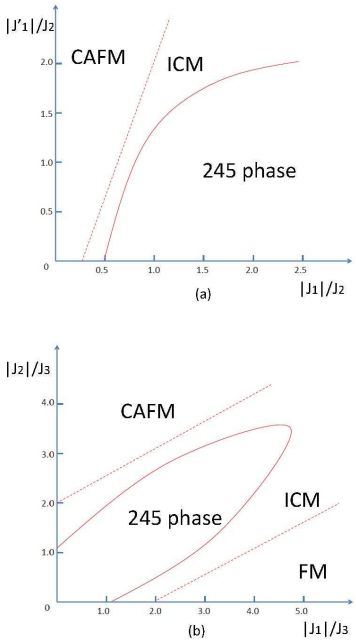

FIG. 8: The phase diagrams against J_1 and J_1' (left) and J_1 and J_2 (right). Solid lines mark second order transitions calculated from spinwave and dotted lines mark possible first order transitions.

phase. An analysis of the spinwave Hamiltonian around Γ point gives us the phase boundary between the 245 magnetic state and ICM as drawn in fig.8. The boundary is set by the equation: $J_1(J_1' + 2(J_e - J_3')) + J_1'(J_2 - J_e + J_3') + 2(J_2(J_e - J_3') + 2J_3(-J_2' + J_3') = 0$. We draw fig.8 (left) for a phase diagram against J_1 and J_1', fixing $J_2 = J_2'$ and $J_3' = 9J_2/20$, and fig.8 (right) for a phase diagram against J_1 and J_2, fixing $J_1' = J_1$, $J_2' = J_2$ and $J_3' = 0$.

Discussion: We have shown that the 245 vacancy pattern can be naturally obtained through saving magnetic energy in a strongly frustrated magnetic model $J_1 - J_2 - J_3$ model. A few remarks regarding our theory need to be addressed. First, in our above analysis, we only consider the magnetic energy and ignore other possible energy sources. In real materials, it is possible that other energy sources may make a significant contribution as well. For example, creating a dimer of two vacancies may cost higher or lower energy than being two individual vacancies. Therefore, comparing a dimer vacancy pattern to a non-dimer pattern requires further careful consideration. The LDA calculation may help to address it[30]. Second, we expect a lattice distortion to naturally take place above or equal to the magnetic transition temperature, similar to what has been observed in iron-pnictides[17]. Third, some LDA calculations have predicted the values of magnetic exchange couplings for $K_2Fe_4As_5$[7]. However, their values are not consistent with our picture. In their results, the NN exchange coupling J_1' is antiferromagnetic and there is no J_3. We expect that both J_1 and J_1' should be FM and J_3 should be significant. Third, it is very important to notice that the NN exchange coupling is strongly ferromagnetic, which contributes the largest energy in the 245 phase. It leads to a high magnetic transition temperature observed in the 245 phase. It is interesting to note that the 245 pattern has also been obtained in one band $t - J - V$ model[31] which is driven by magnetic energy saving in proper parameter regions. Fourth, the ferromagnetic coupling does not contribute to any spin singlet pairing in superconducting (SC) state. Therefore, although the magnetic transition temperature is high in these new materials, we *do not* expect the SC transition temperature can be scaled as the magnetic transition temperature here because the SC transition temperature is determined by the strength of the AFM couplings. Fifth, the SC pairing is mainly determined by J_2[32]. We expect the J_2 value is similar to the one in iron-pnictieds[33, 34] since the SC transition temperatures for both materials are similar. Sixth, the existence of J_3 distinguishes iron-chacogenides from iron-pnictides and generate many different magnetic states. The effect of J_3 in superconducting state will be addressed in a different paper. In fact, J_3 can enhance the s-wave pairing significantly when electron pockets dominate over hole pockets. Finally, the 245 pattern is so strong in magnetism. We do not think this state can be coexisted with superconducting phase.

In summary, the $J_1 - J_2 - J_3$ model provides a natural

and unified understanding for magnetism and vacancy ordering in iron chacogenides. The 245 vacancy pattern reduces the magnetic frustration and achieves the maximum magnetic energy saving. The reduction of frustration increases the ordered magnetic moment as well as strongly enhancing the magnetic transition temperature. (Note, after finishing our paper, we find similar spin-wave excitations for the 245 pattern are calculated and discussed in[35] although the parameters in their model and the physical motivation are very different from us.)

Acknowledgement: JP thanks S. A. Kivelson, Hong Ding, Donglei Feng and X.H. Chen for useful discussion.

[1] J. Guo *et al.*, Phy.Rev.B.82,180520 (2010) **82**, 180520 (2010).
[2] M. Fang *et al.*, ArXiv:1012.5236 (2010).
[3] R. H. Liu *et al.*, ArXiv:1102.2783 (2011).
[4] Y. Zhang *et al.*, Nature Materials DOI:10.1038 (2010).
[5] X. Wang *et al.*, Europhys.Lett. 93,57001 (2011) **93**, 57001 (2011).
[6] D. Mou *et al.*, Phys.Rev.Lett. 106,107001 (2011) **106**, 107001 (2011).
[7] C. Cao and J. Dai, ArXiv:1012.5621 (2010).
[8] L. Zhang and D. J. Singh, Phys.Rev.B 79, 094528 (2009) **79**, 094528 (2009).
[9] X. Yan, M. Gao, Z. LU, and T. Xiang, ArXiv:1012.5536 (2010).
[10] W. Bao *et al.*, ArXiv:1102.0830 (2011).
[11] W. Bao *et al.*, ArXiv:1102.3674 (2011).
[12] J. Bacsa *et al.*, ArXiv:1102.0488 (2011).
[13] V. Y. Pomjakushin *et al.*, ArXiv:1102.1919 (2011).
[14] Z. Wang *et al.*, ArXiv:1101.2059 (2011).
[15] P. Zavalij *et al.*, ArXiv:1101.4882 (2011).
[16] A. M. Zhang *et al.*, ArXiv:1101.2168 (2011).
[17] C. de la Cruz *et al.*, Nature **453**, 899 (2008).
[18] Q. Si and E. Abrahams, Phys. Rev. Lett **101**, 076401 (2008).
[19] C. Fang *et al.*, Phys Rev B **77**, 224509 (2008).
[20] W. Bao *et al.*, arXiv:0809.2058 (2008).
[21] S. Li *et al.*, Phys. Rev. B **79**, , (0)54503 (2009).
[22] F.-C. Hsu *et al.*, PNAS **105**, 14262 (2008).
[23] Y. Mizuguchi *et al.*, Appl. Phys. Lett. **93**, 152505 (2008).
[24] F. Ma *et al.*, Phys. Rev. Lett **102**, 177003 (2009).
[25] C. Fang, B. Andrei Bernevig, and J. Hu, Europhysics Letters **86**, 67005 (2009).
[26] O. J. Lipscombe *et al.*, Phys Rev Lett **106**, 057004 (2011).
[27] P. M. Shiraga *et al.*, Arxiv: 0903.3515 (2009).
[28] X. Li and et al, unpublished .
[29] V. J. Emergy, S. A. Kivelson, and J. M. Tranquada, PNAS **96**, 8814 (1999).
[30] X. Yan, M. Gao, Z. Lu, and T. Xiang, ArXiv:1102.2215 (2011).
[31] S. A. Kivelson, V. J. Emery, and H. Q. Lin, Phy. Rev. B **42**, 6523 (1990).
[32] K. Seo, B. A. Bernevig, and J. Hu, Phys. Rev. Lett **101**, 206404 (2008).
[33] J. Zhao *et al.*, Nature Physics **5**, 55 (2009).
[34] J. Zhao *et al.*, Phys. Rev. Lett. **101**, 167203 (2008).
[35] Y.-Z. You, H. Yao, and D.-H. Lee, arXiv:1103.3884 .